Optical Materials xxx (xxxx) xxx

Contents lists available at ScienceDirect

Optical Materials

journal homepage: http://www.elsevier.com/locate/optmat

The effect of volume inclusions of the $ZnGeP_2$ single-crystal on the dispersion of the refraction index and the absorption coefficient in mid-IR and terahertz ranges of wavelengths

Mikhail Zinoviev [a,c,d,*], Nikolay Yudin [a,c,d], Alexander Gribenyukov [b,d], Sergey Podzyvalov [a,c,d], Victor Dyomin [a], Igor Polovtsev [a], Valentin Suslyaev [a], Yelena Zhuravlyova [a]

[a] National Research Tomsk State University, Tomsk, Russia
[b] Institute of Monitoring of Climatic and Ecological Systems of the Siberian Branch of the Russian Academy of Sciences, Tomsk, Russia
[c] Institute of Atmospheric Optics of Siberian Branch of the Russian Academy of Science, Tomsk, Russia
[d] Laboratory of Optical Crystals, Tomsk, Russia

ARTICLE INFO

Keywords:
THz wavelength range
IR range
Dispersion
$ZnGeP_2$ single-crystal
Volume inclusions
Absorption coefficient

ABSTRACT

Volume filamentary inclusions in $ZnGeP_2$ have been visualized using the digital holography method. The chemical composition of the filamentous volume inclusions Zn_3P_2 and Ge have been determined using the method of X-ray diffraction analysis. It is shown that the presence of volume inclusions in the $ZnGeP_2$ single-crystal leads to an increase in the reflection coefficient in the region of 12.5 μm. The dispersion dependences of the refractive index and the absorption coefficient of the studied $ZnGeP_2$ samples at wavelengths of 300–1000 μm in the region of non-fundamental absorption have been obtained. It has been shown that the presence of volume inclusions in a single-crystal leads to an increase in the refractive index in the entire THz range under study by the value of $\Delta n_{max} = 0{,}0008$. The difference between absorption coefficients for the studied samples varies from $\Delta\alpha = 0.1\ cm^{-1}$ to $\Delta\alpha = 0.15\ cm^{-1}$ depending on the wavelength.

1. Introduction

The progress in development of coherent radiation sources today is largely related to mastering of the terahertz range of wavelengths, as well as the improvement of systems operating in the infrared region of the spectrum. Development of powerful parametric generators of the mid-IR range (2–8 μm) based on $ZnGeP_2$ with an average power of generated radiation of ~100 W and a pulsed energy of ~10 mJ at a pulse repetition rate of ~10 kHz [1], with the possibility of spectral tuning in a wide range of wavelengths, is an intensively developing direction in this field [2]. Another focus of the research is generation at the difference frequency of radiation in the terahertz region of the spectrum with an average power of ~2 mW [3–5]. $ZnGeP_2$ has a high coefficient of nonlinear susceptibility ($\chi^{(2)}$) and an indicator of nonlinear optical quality ($M = \frac{\chi^2}{n^3}$), high thermal conductivity and low absorption ~ 0.04 cm^{-1} at pump wavelengths ($\lambda \sim 2$ μm) and generation in mid-IR and THz ranges. However, a feature of ternary compounds (including $ZnGeP_2$) with a chalcopyrite-type crystalline lattice structure is that the synthesis of a ternary compound occurs as a result of several intermediate reactions. Depending on the temperature and time of the synthesis, in addition to the expected final result (the ternary compound), synthesized ingots have a predetermined number of second phases formed at the mentioned intermediate stages. In particular, the presence of such components as Zn_3P_2, Ge, GeP, and ZnP_2 in the synthesized material during synthesis of the $ZnGeP_2$ compound can be assumed [6]. Deviations from the stoichiometry of the $ZnGeP_2$ compound can be insignificant. However, they appear as an inclusion [7] into the matrix medium with characteristic volume sizes reaching tens and sometimes hundreds of micrometers [8]. Volumetric defects significantly differ in optical properties (refractive index and absorption coefficient) [9,10] from the matrix medium. In this regard, volume defects in a nonlinear crystal lead to violation of phase-matching conditions, which either excludes the possibility of using these elements in optical systems or significantly impairs the efficiency of radiation conversion in such nonlinear media. Such defects destroy the phase synchronism of the

* Corresponding author. National Research Tomsk State University, Tomsk, Russia.
E-mail addresses: muxa9229@gmail.com (M. Zinoviev), rach3@yandex.ru (N. Yudin), alexander.gribenyukov@yandex.ru (A. Gribenyukov), cginen@yandex.ru (S. Podzyvalov), dyomin@mail.tsu.ru (V. Dyomin), polovcev_i@mail.ru (I. Polovtsev), susl@mail.tsu.ru (V. Suslyaev), lenazhura@mail.ru (Y. Zhuravlyova).

https://doi.org/10.1016/j.optmat.2020.110662
Received 8 July 2020; Received in revised form 16 November 2020; Accepted 16 November 2020

propagation of interacting optical waves and reduce the efficiency of nonlinear conversion of the pump frequency to almost zero. This is especially pronounced at a high energy density of the pump radiation of about 2–5 J/cm^2. In addition, inclusions can act as initializers of an optical breakdown of the material.

In [11], using THz spectroscopy methods, it has been shown that absorption of $ZnGeP_2$ in the terahertz region of the spectrum of 300–1000 μm is of diffuse nature, that is, it does not have pronounced resonances in a wide frequency range. By virtue of this fact, an assumption has been made about the decisive role of free carriers in formation of dielectric losses in this frequency range. Studies performed with a variable concentration of free charge carriers under the effect of fast electrons and varying temperature conditions [12,13] have shown the absence of a noticeable effect of temperature (from 300 K to 20 K) on optical parameters of crystals and the absence of a pronounced correlation with post-growth processing conditions (annealing at 600 °C).

In a semiconductor crystal, the interface between the matrix medium and the inclusion of the second phase can manifest itself as a source of free charge carriers. Therefore, spectral effects associated with the presence of second-phase inclusions in $ZnGeP_2$ may appear in the terahertz range. It can be assumed that characteristics of the dispersion spectra of the refractive index and the absorption coefficient in the terahertz region of wavelengths (300–1000 μm) can serve as a basis for identifying the composition of inhomogeneities in the crystal, which can be used for qualitative express determination of the presence and even quantitative estimation of volume defects that affect the generation potential of the crystal in mid-IR and THz ranges. The obtained information can be used to adjust temperature-time parameters of growth and synthesis of the compound in order to increase optical characteristics of nonlinear crystals.

The aim of the paper is to test the aforementioned hypothesis on the dominant effect of second-phase inclusions on quasi-optical characteristics (refractive index and absorption coefficient) in the wavelength range of 300–1000 μm.

2. Experimental samples

The experimental samples used in the work were cut from a $ZnGeP_2$ single-crystal with geometric dimensions of Ø30 × 150 mm (Fig. 1). The single-crystal was grown vertically according to the Bridgman method in the vertical version from a compound previously synthesized using the two-temperature method [7] onto a seed crystal with the orientation (100).

The samples (Fig. 2, a and b) for experimental measurements were cut out along the ingot in the shape of plane-parallel plates oriented parallel to the plane (001) in order to exclude the possible effect of birefringence.

Both plates underwent optical polishing of working surfaces. The thickness of the samples (***d***) was 3600 ± 1 μm. Measurements of the sample thickness were carried out using a micrometric stand with a measurement error of ±1 μm. Thickness control is necessary for a correct measurement of the refractive index.

3. Research techniques

Experimental samples were investigated using digital holography camera (DHC) and X-ray diffraction analysis for the presence of second phases. Using Fourier spectroscopy, the dependence of the reflection coefficient on the wavelength of the test radiation was obtained in the range of 2–13 μm. The dependences of the absorption coefficient and the refractive index on the wavelength were obtained using terahertz spectroscopy. A digital holographic camera (DHC 1.064), manufactured by Laboratory of Optical Crystals, Tomsk, was used for a detailed characterization of samples and visualization of volume defects of the $ZnGeP_2$ single crystal. This camera allows recording holograms and restore the holographic image of the object, which corresponds to a 9 × 12 mm aperture (the limitation is related to final dimensions of the digital camera matrix and its field of view). To register objects that exceed these dimensions, it is necessary to scan the sample using a positioning system, record a set of holograms and their gluing.

The recorded hologram represents the interference field of the reference and object waves transmitted through the sample. This distribution is used as an input in the numerical calculation [14] of the diffraction integral (1) to calculate $U(x_2 y_2)$ – the distribution field in the plane$(x_2 y_2)$, located at a distance Z from the plane of the camera matrix$(x_1 y_1)$:

$$U(x_2, y_2) = \frac{1}{i\lambda z} \int_{-\infty}^{\infty} \int_{-\infty}^{\infty} U\left(x_1, y_1\right) e^{i\frac{2\pi}{4} z} e^{\frac{i\pi}{\lambda z}\left((x_1 - x_2)^2 + (y_1 - y_2)^2\right)} dx_1 dy_1, \quad (1)$$

where λ is the wavelength. Thus, images of crystal layers with an interlayer interval chosen by the operator are numerically restored (calculated), in our case, an interlayer interval of 100 μm). Such a technique can be called a virtual microscope, since the process of displaying the obtained information is similar to the process of longitudinal focusing of a microscope for sharpness. The operation principle, the optical scheme of the DHC, and the visualization technique are examined in detail in Ref. [9,15]. The described method is used to scan the entire crystal volume and perform visualization and presumptive classification of volume defects, determination of their characteristic dimensions and location in three-dimensional space. Currently, this method is successfully used for determination deferent volumetric defects such as cracks, surface scratches, growth striates, needle shaped, drop shaped and comet-shaped inclusions with dimensional sizes from 4 μm [15].

The phase composition of the studied samples was determined at the next stage of the work using X-ray diffraction analysis. The samples were studied on a Rigaku MiniFlex 600 X-ray diffractometer with a Cu X-ray tube at a radiation wavelength of 1.541862 Å. X-ray tube maximum power is 600 W. The diffractometer was equipped with a vertical goniometer with a scanning rate of 10°/min. The minimum goniometer step on a 2Θ scale was 0.005°. The measurements were carried out at a voltage on the x-ray tube of 40 kV and a current of 15 mA. The phase composition analysis was carried out using PDF 4+ database contains more than 444,100 entries of inorganic diffraction data from crystals, as well as the POWDER CELL 2.4 full-profile analysis program. The shooting was carried out in angles of 3° - 60°, in increments of 0.02°.

After determining the phase composition of the samples under study, the spectra of their reflection coefficient in the mid-IR range, as well as the absorption coefficient and the refractive index in the THz range were measured. A Fourier spectrometer FT-801 manufactured by Simex was

Fig. 1. $ZnGeP_2$ single-crystal (30 × 150) grown using the Bridgman method in a vertical version.

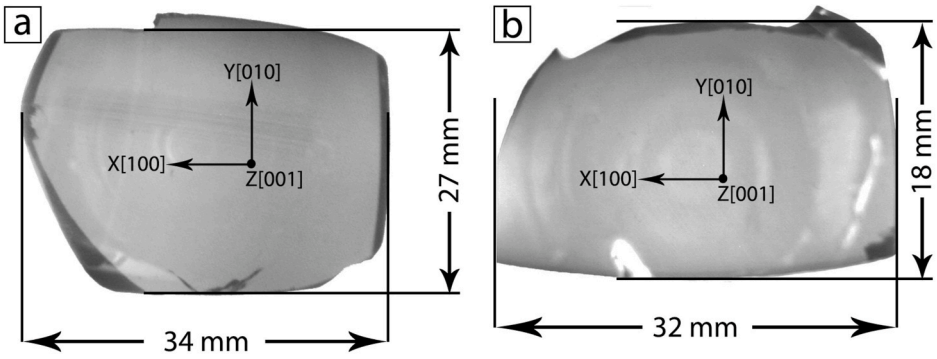

Fig. 2. IR photographs of $ZnGeP_2$ single-crystal plates with printed crystallographic axes (the dot indicates the direction to the reader): the plate with detected defects in the central part (a); the plate without defects (b).

used to record the reflection spectra of the samples under study in the mid-IR region (wavelengths 2–13 μm).

Spectral dependences of the samples in the THz region were obtained using a terahertz spectrometer STD-21. The setup scheme is shown in Fig. 3. The main elements of the system have included THz radiation sources: backward wave tubes (BWT), Mach-Zehnder interferometer, and the Golay cell as a receiver of the system (the setup scheme is described in detail in Ref. [16]). The diameter of the beam of the terahertz emitter collimated using lenses was 10 mm.

All measurements performed in the work were carried out during the propagation of radiation in open space, without the use of waveguides and cooled chambers. Transmission of samples T was determined using formula (2) as the ratio of the power transmitted through the sample P_{sample} to the input power P_0 (radiation in the absence of the sample):

$$T = \frac{P_{sample}}{P_0}. \quad (2)$$

A typical transmission spectrum T has periodic oscillations associated with high transparency of the sample in the terahertz range. These oscillations are associated with multipath interference inside a plane-parallel sample.

In case when the sample under study is sufficiently transparent and periodic oscillations are observed in the transmission spectrum, the main optical characteristics of the material (absorption coefficient and refractive index) can be calculated using formulas of the Fabry-Perot interferometer theory [17]. The distance $\Delta\nu$ between adjacent peaks in the transmission spectrum of the sample is determined by the refractive index of the material, which can be calculated busing formula (3):

$$n(\nu) \sim \frac{c}{\triangle\nu \cdot d}, \quad (3)$$

and the absorption coefficient α is related to the maximum transmittance amplitude T_{rmax} by the following relation (4):

$$\alpha \sim \frac{\ln(T_{r_{max}})}{d}, \quad (4)$$

where, d is the thickness of the sample.

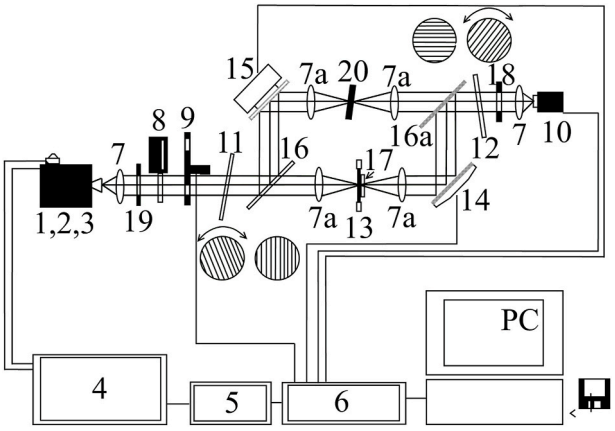

Fig. 3. Schematic representation of the quasi-optical spectrometer STD-21: backward wave tubes (BWT) (1–3); the information processing unit (4–6); fluoroplastic/polyethylene lenses (7, 7a); a set of thin-film attenuators (8); the amplitude modulator (9); the Golay cell (10); the mesh polarizer (11); the mesh analyzer (12); the sample holder (13); the phase modulator (14); the phase compensator (15); the beam splitter (16,16a); the test sample (17); the absorber (18); the absorbing diaphragm (19); the absorber, blocking the second arm of the interferometer (20).

4. Results and discussion

Fig. 4 exhibits a shadow IR image, as well as a hologram and a holographic image reconstructed from a part of a plate that contains volume defects of a filiform shape – sample No. 1.

A shadow IR image (Fig. 4, a) in the $ZnGeP_2$ sample was used to discover regions in which volume inclusions had been observed. Then, based on this data, a hologram of the central part of the plate, where these defects had been detected, was recorded. Since the plate had geometrical dimensions exceeding the field of view of the DHC, the required aperture was synthesized by recording several holograms, one of which is shown in Fig. 4, b. The reconstructed image of the plane, located at a depth of 1.2 mm from the surface of the test plate, is shown in Fig. 4, c. Filaments of inclusions with a thickness of 10 μm and a length of several mm can be observed. Thus, the use of digital holography methods has allowed detecting volume defects inside the $ZnGeP_2$ crystal plate as well as determining their exact location in the sample and characteristic dimensions.

The procedure for recording holograms and their subsequent reconstruction was applied to another plate in which volume defects had not been detected – sample No. 2. The shadow IR image (Fig. 5, a) of the plate, the hologram of its central part (Fig. 5, b), and the reconstructed holographic image (Fig. 5, c) are shown in Fig. 5.

It shall be noted that shadow IR images of both test plates contain a reflection of the lens that is not related to the internal defective structure of the sample. As in the previous experiment, several holograms of the plate No. 2 were recorded using the DHC, and then, holographic images of the plate layers were reconstructed. The reconstructed images (one of which is shown in Fig. 5, c) have shown that there are practically no volume defects in plate No. 2. Only a single local defect with dimensions of ~10 μm has been found in the entire sample volume (in Fig. 5, b and c circled by the red line).

Thus, two samples have been studied using the digital holography method. One of the samples contained a region with a high concentration of filament-like volume defects, and the second sample did not

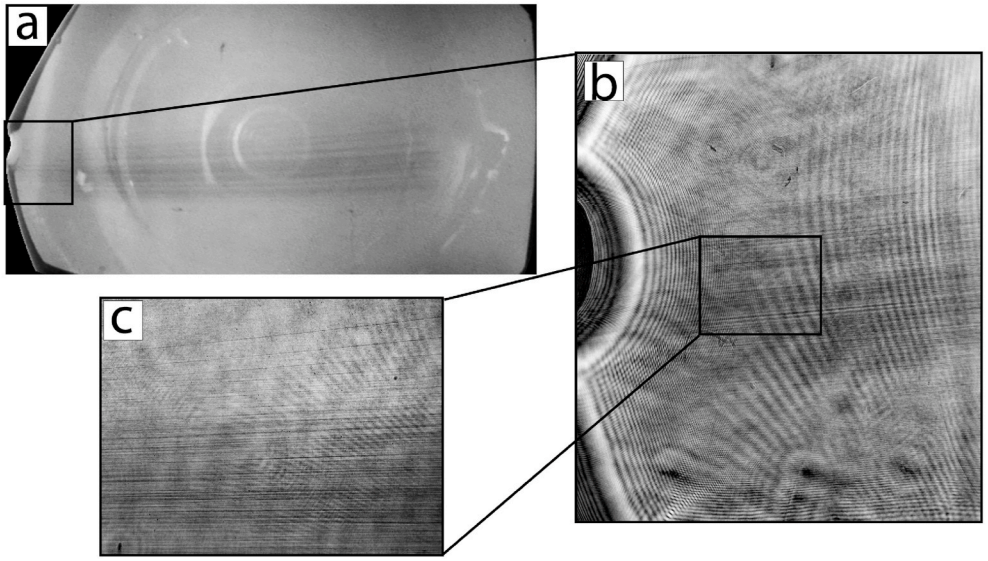

Fig. 4. The shadow IR image of the central part of the investigated plate, in which areas with defects were detected (a); the hologram of a part of the plate obtained with the using DHC (b); the reconstructed image with volume defects in the shape of phosphide filaments located at a depth of 1.2 mm (c).

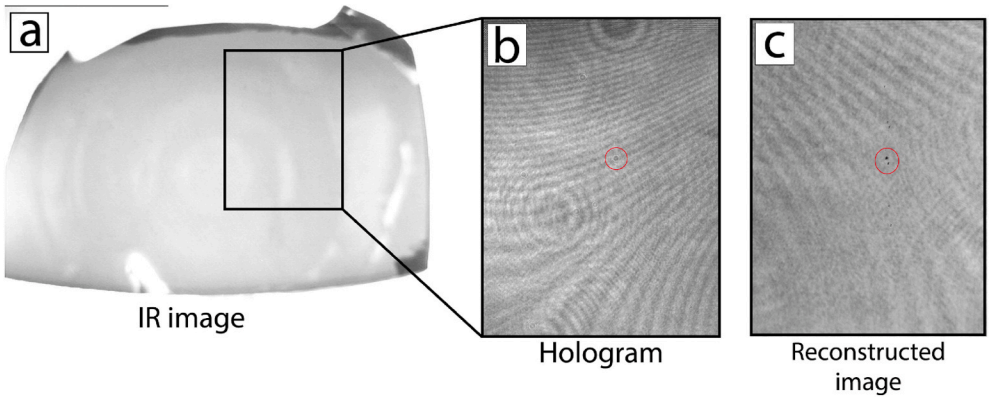

Fig. 5. A shadow IR image of the central part of the investigated plate, in which no defects were detected (a); the hologram of the central part of the plate (b); the reconstructed holographic image (c).

contain accumulation regions of such defects.

Then, an X-ray diffraction analysis of samples No. 1 and No. 2 was carried out. The results of X-ray diffraction analysis are shown in Fig. 6, a, as well as in Table 1. Table 1 exhibits 2-theta (deg) shooting angles, the intensity height (cps), the interplanar spacing ***d*** (ang.), and a compound whose reflexes coincide with sample reflexes (last column). Initially, X-ray reflexes of single-crystal samples No. 1 and No. 2 were recorded. Since the shooting was performed from a single-crystal sample, the reflex of one of the crystalline faces of $ZnGeP_2$ had the maximum intensity. As a rule, reflexes obtained from a single-crystal are much less informative than those from a powder sample, because in the latter case, it is possible to fix reflexes from a larger number of crystalline faces. However, despite this fact, reflexes not related to the $ZnGeP_2$ matrix compound were recorded in the sample No. 1. The results of the X-ray diffraction analysis did not reveal any extraneous phases in the single-crystal sample No. 2. Then, a part of the sample was ground to a powder state. However, recordings of reflexes of the powder sample did not reveal any extraneous phases as well (Fig. 6, b, Table 1).

Reflexes 4 and 6 from sample No. 1 belong to the $ZnGeP_2$ compound from the PDF 4+ database; the remaining reflexes belong to Zn_3P_2, GeP and Ge compounds. The results of the X-ray diffraction analysis has shown that reflexes from the second phases of the intrinsic component, namely, zinc and germanium phosphides were not found in sample No. 2. A comparison of the spectral peaks with the PDF 4+ database has shown that they all belong to the $ZnGeP_2$ compound.

Further studies of samples No. 1 and No. 2 were carried out using methods of IR Fourier spectroscopy and terahertz spectroscopy. Using the IR Fourier spectroscopy method, one of the sides of plane-parallel plates was ground to exclude possible contribution of reflection from the second face of the samples when measuring the reflection coefficient on an IR Fourier spectrometer.

Then, measurements of the IR spectra of the reflection coefficient of samples No. 1 and No. 2 were carried out using a Simex Fourier spectrometer (Fig. 7).

Five measurements have been performed for each sample, average values have been calculated, and measurement errors have been obtained. As can be seen from Fig. 7, the curves of the reflection spectra for samples No. 1 and No. 2 are almost identical in the range of 2–12 μm. A noticeable difference in the reflection spectra is observed in the region of 12–13 μm. A sharp change in the reflection coefficient can be observed in sample No. 2 (Fig. 7, curve 2), as compared to sample No. 1 (Fig. 7, curve 1). In Ref. [18] it was shown that the absorption spectrum of the $ZnGeP_2$ compound contains a resonance absorption band with a wave number of 800 cm^{-1} (12.5 μm), which causes a change in the absorption coefficient and the refractive index. Since the refractive index is related to the reflection coefficient by the relation (5):

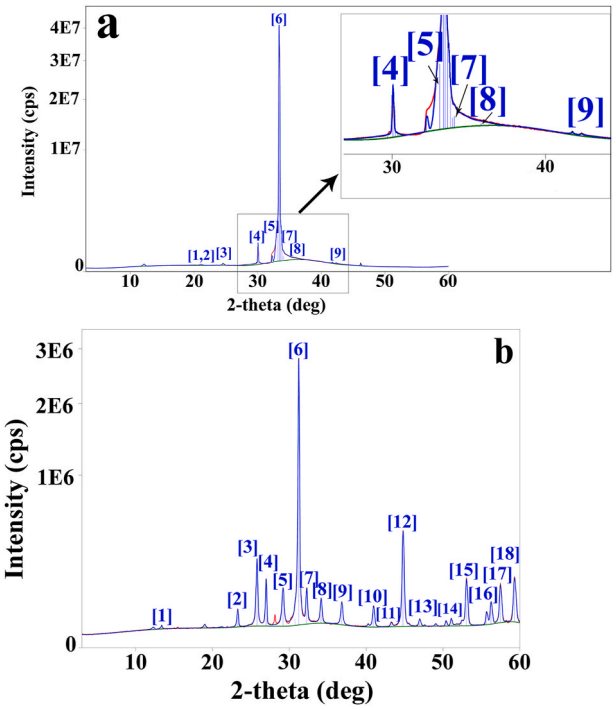

Fig. 6. The X-ray spectrum of the sample No. 1 containing needle-shaped inclusions (a); the X-ray spectrum of the sample No. 2 without needle-shaped inclusions (b).

$$R = \left(\frac{n_1 - n_2}{n_1 + n_2}\right)^2, \tag{5}$$

its change is indirectly reflected in the spectrum of the reflection coefficient (curve 2). Indeed, a sharp change in the refractive index is observed in the region of 12.5 μm due to the resonance absorption band in $ZnGeP_2$, and the graph of the dependence of R on the wavelength for a "pure" sample (curve 2, Fig. 7) also exhibits a sharp change in the curve. Since volume defects differ in the value of the refractive index from the matrix medium, in sample No. 1 in the region of 12–12.5 μm we have a different behavior of the spectral curve of the reflection coefficient (there is no sharp decline).

Curve 1 in Fig. 7 characterizes the behavior of the reflection spectrum of the sample containing volume defects. The spectrum of the given sample is characterized by the fact that it decreases monotonically in the region of 12–13 μm wavelengths, but there is no sharp decrease in the reflection coefficient associated with the resonance absorption band. Thus, the resonance absorption band of $ZnGeP_2$ in the region of 12–12.5 μm can serve as an informative marker for the absence of volume inclusions of Zn_3P_2 and Ge. However, it is important to note that the absorption band of 12–12.5 μm is weak enough to detect small accumulations of volume defects.

The absorption dispersion, according to Ref. [18], in the wavelength range of 100–1000 μm has the shape of a monotonically decreasing curve, and this region includes a region of non-fundamental absorption with no resonances in the spectral curve. The measured transmittance values of the studied samples in the terahertz region of the spectrum (300–1000 μm) on a THz installation STD-21 were used to calculate the refractive index and the absorption coefficient in the T-scan software according to formulas (3), (4), and the approximation of the calculated points with lines were made on the basis of the Sellmeier formulas (6), (7) [19]:

$$n_o^2(\lambda) = 4.47330 + \frac{5.26576\lambda^2}{\lambda^2 - 0.13381} + \frac{1.49085\lambda^2}{\lambda^2 - 662.55}, \tag{6}$$

Table 1
The interpretation of the X-ray spectrum peaks of sample No. 1 and sample No. 2

sample	N⁰	2-theta (deg)	d (Å)	Height (cps)	Phase name
N⁰1	1	20.67 (6)	4.294 (13)	1686 (119)	Zinc Phosphide (1,1,-1)
	2	21.124 (14)	4.202 (3)	4756 (199)	Zinc Phosphide (2,0,0)
	3	24.559 (12)	3.6219 (17)	11,225 (306)	Zinc Phosphide (2,1,0)
	4	29.71 (13)	3.005 (12)	7542 (251)	Germanium Zinc Phosphide (1,1,1)
	5	33.10 (6)	2.704 (5)	869,214 (2691)	Zinc Phosphide (2,2,0)
	6	33.3633 (8)	2.68346 (6)	32,906,254 (16,560)	Germanium Zinc Phosphide (2,0,0)
	7	34.07 (11)	2.630 (8)	84,183 (838)	Zinc Phosphide (2,2,-1), Germanium Phosphide (2,1,1)
	8	35.8 (8)	2.51 (5)	17,233 (379)	Zinc Phosphide (0,2,2)
	9	42.256 (13)	2.1370 (6)	6240 (228)	Zinc Phosphide (1,3,1), Germanium Phosphide (3,0,0)
N⁰2	1	18.301 (12)	4.844 (3)	700 (26)	Germanium Zinc Phosphide (1,0,1)
	2	28.539 (2)	3.1251 (3)	156,985 (396)	Germanium Zinc Phosphide (1,1,2)
	3	32.8199 (15)	2.72663 (12)	18,929 (138)	Germanium Zinc Phosphide (2,0,0)
	4	33.527 (3)	2.6707 (2)	6084 (78)	Germanium Zinc Phosphide (0,0,4)
	5	47.0676 (10)	1.92917 (4)	50,752 (225)	Germanium Zinc Phosphide (2,2,0)
	6	47.5945 (7)	1.90903 (2)	98,848 (314)	Germanium Zinc Phosphide (2,0,4)
	7	55.9401 (15)	1.64239 (4)	74,641 (273)	Germanium Zinc Phosphide (3,1,2)
	8	56.8591 (13)	1.61801 (3)	28,042 (167)	Germanium Zinc Phosphide (1,1,6)
	9	58.978 (2)	1.56482 (5)	7261 (85)	Germanium Zinc Phosphide (2,2,4)
	10	68.7072 (9)	1.365051 (16)	13,586 (117)	Germanium Zinc Phosphide (4,0,0)
	11	70.3417 (13)	1.33728 (2)	4787 (69)	Germanium Zinc Phosphide (0,0,8)
	12	75.9825 (12)	1.251414 (17)	14,552 (121)	Germanium Zinc Phosphide (3,3,2)
	13	76.7626 (15)	1.24063 (2)	26,448 (163)	Germanium Zinc Phosphide (3,1,6)
	14	78.217 (3)	1.22115 (3)	2943 (54)	Germanium Zinc Phosphide (4,2,0)
	15	78.611 (3)	1.21603 (4)	2848 (53)	Germanium Zinc Phosphide (4,0,4)
	16	79.770 (7)	1.20124 (9)	1925 (44)	Germanium Zinc Phosphide (2,0,8)
	17	87.787 (4)	1.11102 (4)	26,406 (162)	Germanium Zinc Phosphide (4,2,4)
	18	89.36 (7)	1.0955 (7)	11,503 (107)	Germanium Zinc Phosphide (2,2,8)

$$n_e^2(\lambda) = 4.63318 + \frac{5.34215\lambda^2}{\lambda^2 - 0.14255} + \frac{1.45795\lambda^2}{\lambda^2 - 662.55}. \tag{7}$$

Fig. 8 exhibits spectra characterizing the dispersion of the refractive index of the studied plates of the $ZnGeP_2$ single-crystal with (1) and without (2) detected inclusions. The spectra of refractive indices for both samples have a monotonically decreasing nature with increasing wavelength of the radiation incident on the sample. From the side of the short-wavelength region of the obtained spectral characteristic, the difference in values of the refractive index between curves 1 and 2 is equal to $\Delta n = 0{,}0008$. With an increase in the wavelength from up to 1000 μm, the difference is equal to $\Delta n = 0.0006$. The average values of the refractive index obtained during the experiment, as well as the shape of dispersion curves, correlate with the data obtained in Ref. [20].

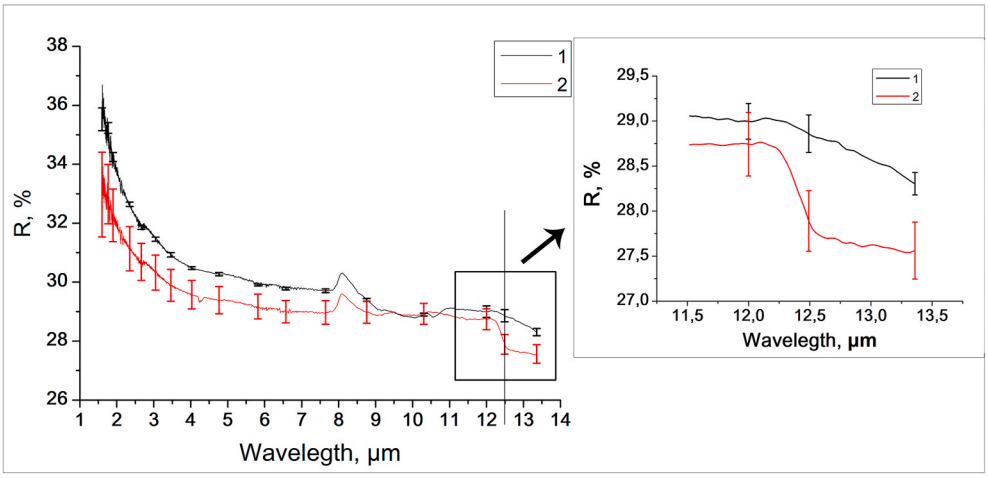

Fig. 7. Sample reflection spectra obtained using a Fourier spectrometer: the sample containing volume inclusions (curve 1); the "pure" $ZnGeP_2$ sample without inclusions (curve 2).

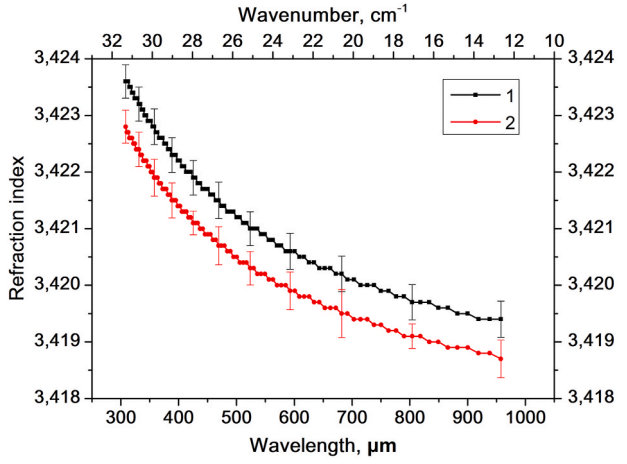

Fig. 8. The dependence of the refractive index on the wavelength: for the plate with detected volume inclusions (curve 1); for the "pure" $ZnGeP_2$ plate (curve 2).

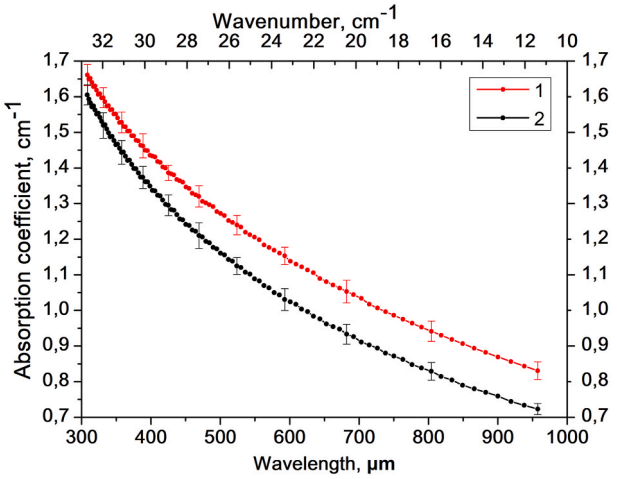

Fig. 9. Absorption coefficient spectra of the studied samples: for the plate with detected volume inclusions (curve 1); for the "pure" $ZnGeP_2$ plate (curve 2).

Formula (3) has been differentiated to analyze the measurement error in the refractive index, and formula (8) has been obtained:

$$\Delta n = \frac{1}{2}\frac{c}{\Delta\nu}\frac{\Delta d}{d}, \tag{8}$$

where $\Delta\nu$ is the distance on the frequency curve between interference maxima, c is the speed of light, d is the nominal thickness of the sample, Δd is the deviation from the nominal thickness. Given that d = 3.6 mm (3600 μm), and Δd is the value ± 1 μm, we obtain $\frac{\Delta d}{d} = 0{,}0003$. Thus, a change in the plate thickness by 1 μm entails a change in the refractive index of the plate by $\Delta n = 0.0003$. The difference in refractive indices for spectra 1 and 2 is Δn from 0.0006 to 0.0008, depending on the selected wavelength region, and exceeds the measurement error from the thickness by a factor of 2. Consequently, the presence of volume defects of the second phase Zn_3P_2, as well as Ge that did not react during synthesis in the sample, causes a difference in average refractive indices of the presented spectra. A change in the composition of the substance in the irradiated region, namely, the presence of Zn_3P_2 and Ge in the sample, leads to an increase in the refractive index of the single-crystal compound $ZnGeP_2$, as shown in Fig. 8. A similar effect was demonstrated in Ref. [21], where it was shown that impurities can significantly affect the value of the semiconductor refraction index.

Absorption coefficient spectra of the studied samples (presented in Fig. 9) have been obtained in the wavelength range of 300–1000 μm.

Curves 1 and 2 characterize the dispersion of absorption coefficients [22] of sample No. 1, and sample No. 2, respectively. It can be seen from the obtained data that volume inclusions Zn_3P_2 and Ge make an additional contribution to the absorption of the sample in the wavelength range of 300–1000 μm (curve 1). The difference in absorption coefficients for the two samples reaches $\Delta\alpha = 0.15$ cm^{-1}. In the short-wavelength region of wavelengths (≤350 μm), the difference in absorption coefficients of sample No. 1 and No. 2 decreases, $\Delta\alpha$ becomes ≤0.1 cm^{-1}, which, apparently, is related to approaching the wavelength region that contains a resonance absorption band (closest with $\lambda = 83.3$ μm). Thus, the range of 300–1000 μm wavelengths is a characteristic range where these inclusions show a noticeable effect on the spectrum.

5. Conclusion

Volume filamentary inclusions in $ZnGeP_2$ have been visualized using the digital holography method. Their characteristic dimensions and their location in the sample volume have been determined.

The chemical composition of the filamentous volume inclusions Zn_3P_2 and Ge have been determined using the method of X-ray diffraction analysis.

The fact of the effect of second-phase inclusions (Zn_3P_2 and Ge) on

quasi-optical characteristics (refractive index and absorption coefficient) in the resonance absorption band (12–12.5 μm) has been established. The presence of volume inclusions in the $ZnGeP_2$ single-crystal leads to an increase in the reflection coefficient in the region of 12.5 μm. It has been shown that the spectral dependence of the reflection coefficient in the resonance absorption band of $ZnGeP_2$ in the range of 12–12.5 μm is an informative marker for the presence of volume inclusions Zn_3P_2 and Ge. However, the relative difference between the obtained spectral characteristics at a wavelength of 12.5 μm is about 5% therefore, this method has low detection ability.

The dispersion dependences of the refractive index and the absorption coefficient of the studied $ZnGeP_2$ samples at wavelengths of 300–1000 μm in the region of non-fundamental absorption have been obtained. It has been shown that the presence of volume inclusions in a single-crystal leads to an increase in the refractive index in the entire THz range under study by the value of = 0,0008. This fact also indirectly confirms the assumption that the presence of volume defects in a crystal can lead to a failure of phase matching conditions when generating THz radiation with a wavelength of ~100–1000 μm at a difference frequency (the wavelength range where the maximum average power of the generated THz radiation in a nonlinear $ZnGeP_2$ crystal was obtained). Moreover, a dispersion of the absorption coefficient has been obtained in this spectral range. The difference between absorption coefficients for the studied samples varies from $\Delta\alpha = 0.1$ cm^{-1} to $\Delta\alpha = 0.15$ cm^{-1} depending on the wavelength. A decrease in the difference between average values on the spectral curves is associated with an approach to the anomalous dispersion region — resonance absorption bands with $\lambda = 83.3$ μm.

The obtained experimental results confirm the assumption about the decisive role of free carriers in formation of dielectric losses in the wavelength range of 100–1000 μm. The hypothesis that the interface between the matrix medium and the inclusion of the second phase is one of the main sources of free carriers in $ZnGeP_2$ has been confirmed. The effect of second-phase inclusions on quasi-optical characteristics (refractive index and absorption coefficient) in the non-fundamental absorption region for wavelengths of 300–1000 μm has been established.

The described methods based on a comparison of spectral characteristics in mid-IR and THz ranges can be used for non-contact rapid diagnostics of single-crystals for the presence of volume inclusions Zn_3P_2 and Ge and a preliminary and non-destructive assessment of the optical strength of the material, which requires an integral characterization of all inclusions due to the probabilistic nature of the optical breakdown.

The technique described in this work by the example of a $ZnGeP_2$ single crystal for visualizing volumetric defects and determining their location in the sample volume using the digital holography method and simultaneous determination of the chemical composition using X-ray diffraction analysis can be used to determine volumetric inclusions not only $ZnGeP_2$ but also other new multicomponent single crystals such as $BaGa_4Se_7$, $BaGa_2GeSe_6$, Li_2ZnGeS_4 [23,24] in order to increase their optical quality. At the moment, the issues of defect formation and an increase their optical breakdown threshold of these single crystals are being intensively studied [24–26].

Funding

This research was supported by "The Tomsk State University competitiveness improvement program" under Academician D.I. Mendeleev Fund Program.

Availability of data and material

All material in the present paper has open access and is not contained unavailable information.

CRediT authorship contribution statement

Mikhail Zinoviev: Experimental work, Methodology, Formal analysis, Writing - original draft. **Nikolay Yudin:** Experimental work, Methodology, Data curation, Writing, Investigation. **Alexander Gribenyukov:** Data curation, Writing - review editing. **Sergey Podzyvalov:** Experimental work, Formal analysis, Writing - review editing. **Victor Dyomin:** Supervision, Writing - review editing. **Igor Polovtsev:** Supervision, Validation, Writing - review editing. **Valentin Suslyaev:** Writing - review editing. **Yelena Zhuravlyova:** Experimental work, Writing - review editing.

Declaration of competing interest

The authors declare that they have no known competing financial interests or personal relationships that could have appeared to influence the work reported in this paper.

Acknowledgments

This research was supported by "The Tomsk State University competitiveness improvement program" under Academician D.I. Mendeleev Fund Program.

References

[1] Q. Chuan-Peng, Y. Bao-Quan, Zh Ben-Rui, L. Gao-You, D. Xiao-Ming, Y. Tong, J. You-Lun, W. Yue-Zhu, High repetition rate 102 W middle infrared $ZnGeP_2$ master oscillator power amplifier system with thermal lens compensation, Opt. Lett. 44 (2019) 715–718, https://doi.org/10.1364/OL.44.000715.

[2] G. Stoeppler, N. Thilmann, V. Pasiskevicius, A. Zukauskas, C. Canalias, M. Eichhorn, Tunable Mid-infrared $ZnGeP_2$ RISTRA OPO pumped by periodically-poled Rb:KTP optical parametric master-oscillator power amplifier, Optic Express 20 (2012) 4509–4517, https://doi.org/10.1364/OE.20.004509.

[3] A.A. Sirotkin, N.N. Yudin, V.V. Dyomin, A.I. Gribenyukov, Tunable THz-radiation in a $ZnGeP_2$ single crystal pumped by dual-wavelength degenerate optical parametric oscillator, Laser Phys. Lett. 17 (2020), 035402, https://doi.org/10.1088/1612-202X/ab72a0.

[4] D. Creeden, J.C. McCarthy, P.A. Ketteridge, T. Southward, P.G. Schunemann, J. J. Komiak, W. Dove, E.P. Chicklis, Compact fiber-pumped terahertz source based on difference frequency mixing in ZGP, IEEE J. Sel. Top. Quant. Electron. 13 (2007) 732–737, https://doi.org/10.1109/JSTQE.2007.896569.

[5] G.K. Kitaeva, Terahertz generation by means of optical lasers, Laser Phys. Lett. 5 (2008) 559–576, https://doi.org/10.1002/lapl.200810039.

[6] A.I. Gribenyukov, S.M. Vatnik, V.V. Dyomin, S.N. Podzyvalov, I.G. Polovtsev, N. N. Yudin, Energy and spectral characteristics of a parametric generator based on a nonlinear $ZnGeP_2$ crystal pumped by a Ho:YAG laser, Quant. Electron. 48 (2018) 603–606, https://doi.org/10.1070/QEL16682.

[7] G.A. Verozubova, A.I. Gribenyukov, YuP. Mironov, Two-temperature synthesis of $ZnGeP_2$, Inorg. Mater. 43 (2007) 1040–1045, https://doi.org/10.1134/S0020168507100020.

[8] G.A. Verozubova, A.O. Okunev, A.I. Gribenyukov, A.Yu Trofimiv, E.M. Trukhanov, A.V. Kolesnikov, Growth and defect structure of $ZnGeP_2$ crystals, J. Cryst. Growth 312 (2010) 1122–1126, https://doi.org/10.1016/j.jcrysgro.2009.11.009.

[9] V. Dyomin, A. Gribenyukov, S. Podzyvalov, N. Yudin, M. Zinoviev, I. Polovtsev, A. Davydova, A. Olshukov, Application of infrared digital holography for characterization of inhomogeneities and voluminous defects of single crystals on the example of $ZnGeP_2$, Appl. Sci. 10 (2020) 442, https://doi.org/10.3390/app10020442.

[10] P.I. Baransky, V.P. Klochkov, I.V. Potykevich, Semiconductor Electronics, 1975 (in Russian), Kyiv.

[11] V.V. Voicehovsky, A.A. Volkov, G.A. Komandin, YuA. Shakir, Dielectric properties of $ZnGeP_2$ in far IR-range of wavelengths, Phys. Solid State 37 (1995) 2199–2202.

[12] S.V. Chuchupal, G.A. Komandin, E.S. Zhukova, O.E. Porodinkov, I.E. Spektor, A. I. Gribenyukov, Effect of electron irradiation of $ZnGeP_2$ single crystals on terahertz losses in a wide temperature range, Phys. Solid State 57 (2015) 1607–1612, https://doi.org/10.1134/s1063783415080041.

[13] A.I. Gribenyukov, K. V Dorozhkin, A.N. Morozov, V.I. Suslyaev, Influence of after-growth treatments on the optical parameters of terahertz $ZnGeP_2$ crystals, Russ. Phys. J. 60 (2018) 2000–2003, https://doi.org/10.1007/s11182-018-1314-9.

[14] V. Dyomin, I. Polovtsev, D. Kamenev, Quality control of $ZnGeP_2$ single crystals using optical methods, Russ. Phys. J. 58 (2016) 1479–1481, https://doi.org/10.1007/s11182-016-0672-4.

[15] V. Dyomin, A. Gribenyukov, A. Davydova, M. Zinoviev, A. Olshukov, S. Podzyvalov, I. Polovtsev, N. Yudin, Holography of particles for diagnostics tasks [Invited], Appl. Optic. 58 (2019) G300–G310, https://doi.org/10.1364/AO.58.00G300.

[16] E.V. Emelyanov, V.I. Suslyaev, G.E. Dunaevskii, V.A. Zhuravlev, V.L. Kuznetsov, S. I. Moseenkov, I.N. Mazov, Terahertz transmission spectra of composite materials based on MWNT with different time of ultrasonic processing, IRMMW-THz (2012) 1–2, https://doi.org/10.1109/IRMMW-THz.2012.6380147.

[17] J.M. Vaughan, The Fabry-Perot Interferometer: History, Theory, Practice and Applications, first ed., Taylor & Francis, New York, 1989.

[18] S.V. Chuchupal, G.A. Komandin, E.S. Zhukova, A.S. Prokhorov, O.E. Porodinkov, I. E. Spektor, Yu A. Shakir, A.I. Gribenyukov, Mechanisms of loss formation in nonlinear optical crystals $ZnGeP_2$ in the terahertz frequency range, Phys. Solid State 56 (2014) 1391–1396, https://doi.org/10.1134/S1063783414070063.

[19] D. Nikogosyan, Handbook "Nonlinear Optical Crystals: A Complete Survey,", first ed., Springer, New York, 2005.

[20] V.V. Apollonov, A.I. Gribenyukov, V.V. Korotkova, A.G. Suzdaltsev, YuA. Shakir, Subtraction of the CO_2 laser radiation frequencies in a $ZnGeP_2$ crystal, Quant. Electron. 23 (1996) 469–470, https://doi.org/10.1070/QE1996v026n06ABEH000701.

[21] D.A. Pashkeev, YuG. Selivanov, E.G. Chizhevskii, D.B. Stavrovskii, I.I. Zasavitskiy, Dispersion of the refractive index of epitaxial $Pb_{1-x}Eu_xTe$ ($0 <= x <= 1$) alloy layers below the absorption edge, Semiconductors 45 (2011) 980–987, https://doi.org/10.1134/S1063782611080148.

[22] A.I. Gribenyukov, V.I. Voevodin, Influence of the preparation conditions on optical properties of single crystals $ZnGeP_2$ in THz range, IOP Conf. Series: J. Phys. Conf. (2018), 052030, https://doi.org/10.1088/1742-6596/1115/5/052030, 1115.

[23] X. Lin, Y. Guo, N. Ye, $Baga_2GeX_6$(X=S, Se): new mid-IR nonlinear optical crystals with large band gaps, J. Solid State Chem. 195 (2012) 172–177, https://doi.org/10.1016/j.jssc.2012.01.043.

[24] I. Huang, K. Wu, J. Cheng, Y. Chu, Z. Yang, S. Pan, Li_2ZnGeS_4: a promising diamond-like infrared nonlinear optical material with high laser damage threshold and outstanding second-harmonic generation response, Dalton Trans. 48 (2019) 4484–4488, https://doi.org/10.1039/C9DT00269C.

[25] N.Y. Kostyukova, A.A. Boyko, E.Y. Erushin, A.I. Kostyukov, V.V. Badikov, D. V. Badikov, D.B. Kolker, Laser-induced damage threshold of $Baga_4Se_7$ and $Baga_2GeSe_6$ nonlinear crystals at 1.053 μm, J. Opt. Soc. Am. B: Opt. Phys. 36 (2019) 2260–2265, https://doi.org/10.1364/JOSAB.36.002260.

[26] N.Yu Kostyukova, A.A. Boyko, I.D. Eranov, O.L. Antipov, D.B. Kolker, A. I. Kostyukov, E.Yu Erushin, I.B. Miroshnichenko, D.V. Badikov, V.V. Badikov, Laser-induced damage threshold of the nonlinear crystals $Baga_4Se_7$ and $Baga_2GeSe_6$ at 2091 nm in the nanosecond regime, J. Opt. Soc. Am. B: Opt. Phys. 37 (2020) 2655–2659, https://doi.org/10.1364/JOSAB.396746.